Nano Today 43 (2022) 101399

Contents lists available at ScienceDirect

Nano Today

journal homepage: www.elsevier.com/locate/nanotoday

Self-powered photodetector for ultralow power density UV sensing

Jianping Meng[a,b], Qi Li[a,c,d], Jing Huang[a,c,d], Caofeng Pan[a,b,c], Zhou Li[a,b,c,*]

[a] CAS Center for Excellence in Nanoscience, Beijing Key Laboratory of Micro–Nano Energy and Sensor, Beijing Institute of Nanoenergy and Nanosystems, Chinese Academy of Sciences, Beijing 101400, China
[b] School of Nanoscience and Technology, University of Chinese Academy of Sciences, Beijing 100049, China
[c] Center on Nanoenergy Research, School of Physical Science and Technology, Guangxi University, Nanning 530004, China
[d] College of Chemistry and Chemical Engineering, Guangxi University, Nanning 530004, China

ARTICLE INFO

Article history:
Received 17 December 2021
Received in revised form 12 January 2022
Accepted 13 January 2022
Available online 19 January 2022

Keywords:
Self-powered
Localized surface plasmon resonance
Pyro-phototronic effect
Photodetector

ABSTRACT

Ultralow power density UV sensing is crucial to application in military and civilian fields. However, it is still confronted with a low signal-to-noise ratio and long response/recovery time. Here, we report a self-powered photodetector based on the Schottky junction of Au NPs@ZnO NWs, which can detect 325 nm light with the power density of 68 nW/cm^2, by using pyro-phototronic effect enhanced by localized surface plasmon resonance (LSPR). Under the illumination of 325 nm with the power density of 68 nW/cm^2, responsivity of photodetector dramatically enhances from 0 to 0.485 mA/W after decorating Au NPs, detectivity is boosted from 0 to 27.49 × 10^{10} Jones. The responsivity and detectivity of self-powered photodetector show significant enhancement of over 3290% and over 3298% under the illumination of 325 nm light with the power density of 170 nW/cm^2. The fast recovery ensure detection can be finished within 12 ms. The coupled effect of pyroelectric effect and LSPR provides a guideline to design a high-performance photodetector using other nanomaterials.

Introduction

Ultraviolet (UV) detection is crucial for potential application in defense warning systems of military, flame warning, environmental monitoring, UV communication, flame sensing, environmental monitoring, space science, life science [1–4]. Metal-oxide semiconductor-based photodetector attracts plenty of attention benefiting from easy fabrication and excellent robustness for radiations and severe environment [5,6]. As a typical metal-oxide semiconductor, wide bandgap ZnO nanowire (NW) is desired candidate because of the suitable bandgap (3.37 eV), large surface-to-volume ratio, low-cost [7–9]. Besides, the small electron and hole collision ionization coefficient, high exciton binding energy of 60 meV at room temperature, and environmental friendliness endow the ZnO more attention in the field of photodetection [10–12]. Generally, ZnO NWs based photodetector also forms a p-n junction[13] or Schottky junction [14] to suppress dark current and improve the signal to noise ratio. Additionally, the photovoltaic effect in the built-in potential of the junction is beneficial for the separation of photogenerated electron-hole pairs, it endows the features of self-powered detection without consuming external power [15–17]. The self-powered photodetector can detect or monitor the ambient light by converting the incident light into a measurable electrical signal, which is significant for the distributed photodetector as portable/wearable devices [18,19].

ZnO NWs based photodetector with a p-n junction or Schottky junction exhibits high sensitivity for UV light without a bias voltage. However, the native point defect of oxygen vacancy located within the bandgap of ZnO leads to the persistent photoconductive (PPC) effect [20–24], especially under the illumination of short-wavelength light [25,26]. It degrades the recovery time of the ZnO NW-based UV sensors. Applying a short-duration (~ns or ~ms) positive voltage pulse can suppress the PPC by inducing the electron accumulation at the surface of oxide semiconductor and recombination with ionized oxygen vacancy sites [20,24]. This increases the complexity of photodetector and impedes self-powered detection. For pyroelectric semiconductor of ZnO NWs with non-centrosymmetric crystal structures, the transient pyro-potential from the light-induced change of spontaneous polarization can shorten the response and recovery time significantly due to time-dependently changing temperature across the semiconductors once UV light illuminates [2,27–30], which can suppress the PPC effectively. This working mechanism is called the light-induced pyro-phototronic effect

* Corresponding author at: CAS Center for Excellence in Nanoscience, Beijing Key Laboratory of Micro–Nano Energy and Sensor, Beijing Institute of Nanoenergy and Nanosystems, Chinese Academy of Sciences, Beijing 101400, China.
E-mail address: zli@binn.cas.cn (Z. Li).

https://doi.org/10.1016/j.nantod.2022.101399
1748-0132/

[11,30,31]. Whereas low photothermal conversion efficiency of UV light causes weak pyroelectric potential, especially for UV light with low power density. High-sensitive detection of UV light with low power density is important in defense warning systems of the military. It extends the warning range to gain defense time.

Pyroelectric current is dependent on the rate of temperature change for ZnO NW under the illumination of UV light. Two strategies have been developed to increase the rate of temperature change: (i) improving photothermal conversion of UV light with low power density; and (ii) decreasing substrate temperature [32]. Whereas the second strategy limits the application of photodetector at room temperature or high temperature. Here, we choose the first strategy to enhance the pyroelectric current of ZnO NW-based photodetector by localized surface plasmon resonance (LSPR). LSPR can produce transient thermal power once UV light illuminates on a metal nanoparticle, which can enhance the light-induced heating effect and light absorptance [33–37]. This transient high-temperature is widely used in welding [38], photothermal therapy of cancer [39], improvement of photovoltaic devices [40], and so on. Our strategy is the enhancement of photo responsivity to UV light with low power density by coupling with the LSPR and pyro-phototronic effect. When a metal nanoparticle is illuminated by UV light which has highly energetic photons, plasmonic hot-electrons produced by LSPR can escape from the metal nanoparticle and be collected by a semiconductor at the metal-semiconductor interface of Schottky junction, which can enhance photocurrent [41]. It endows an additional superior to our strategy.

In our work, a self-powered photodetector is prepared by forming a Schottky junction of ZnO NWs to detect UV light with low power density. The performance of the self-powered photodetector is reinforced by decorating Au nanoparticles (NPs) on the surface of ZnO NWs, including responsivity, detectivity, response time, and recovery time. The self-powered photodetector can realize the detection of UV light of 68 nW/cm^2. Meanwhile, the response/recovery time is about 15 ms. This simple and ingenious method opens up the possibility to develop a high-performance photodetector in the detection of UV light with low power density.

Results and discussion

The structures of materials and photodetector are illustrated in Fig. 1. ZnO NWs are synthesized by the hydrothermal method. Then, Au NPs are decorated on the surface ZnO NWs by sputtering the Au target (Fig. 1a). The length and diameter of ZnO NW are ~ 10 μm and ~ 100 nm (Fig. 1b and Fig. S2a), and hexagon morphology can be observed from the top view (Fig. 1b). XRD pattern confirms that ZnO NWs are grown along the *c*-axis preferentially (Fig. S1). Interplanar distance of 0.259 nm is verified from the high-resolution TEM (HRTEM) image, which is assigned to the panels of *h*-ZnO(002) (Fig. S2b). Proofs of selected area electron diffraction (SAED) and energy dispersive spectroscopy (EDS) certify the nature of single crystal and composition of ZnO NWs (Fig. S2c-f). ZnO NWs after decorating Au NPs with a loading amount of 46.2 nmol/cm^2 are used for TEM characterization. The radius of Au NPs prepared by the sputtering method is ~ 3 nm from the TEM image (Fig. 1c). The interplanar distance from an inset image of the HRTEM image (Fig. 1d) is 0.236 nm, which corresponds to Au (111). It provides evidence that Au NPs have been decorated on the surface of ZnO NWs. Further proof of Au NPs is observed from the EDS spectrum (Fig. S3). The nanoscale of Au NPs can suppress the scattering effect and enhance the absorption effect of incident UV light [42]. It is beneficial to enhance the photothermal conversion inducted by LSPR. X-ray photoelectron spectroscopy (XPS) and photoluminescence (PL) spectra are used to confirm the state of oxygen vacancies for ZnO NWs before and after decorating Au NPs. In O 1 s spectra (Fig. 1e), two peaks can be observed from the deconvolution results of O 1 s for initial ZnO NWs and ZnO NWs after decorating Au NPs of 46.2 nmol/cm^2. The peaks at 531.7 eV and 530.2 eV are attributed to the O atoms in the vicinity of oxygen vacancies and O-Zn bond, respectively [43]. The integral-area ratios of the perk at 531.7 eV to the peak at 530.2 eV are 0.588 and 0.385 for original ZnO NWs and ZnO NWs after decorating Au NPs of 46.2 nmol/cm^2, indicating the decrease or passivation of oxygen vacancies in the surface of ZnO by decorating Au NPs on ZnO NWs. Photoluminescence (PL) spectra of initial ZnO NWs and ZnO NWs after decorating Au NPs of

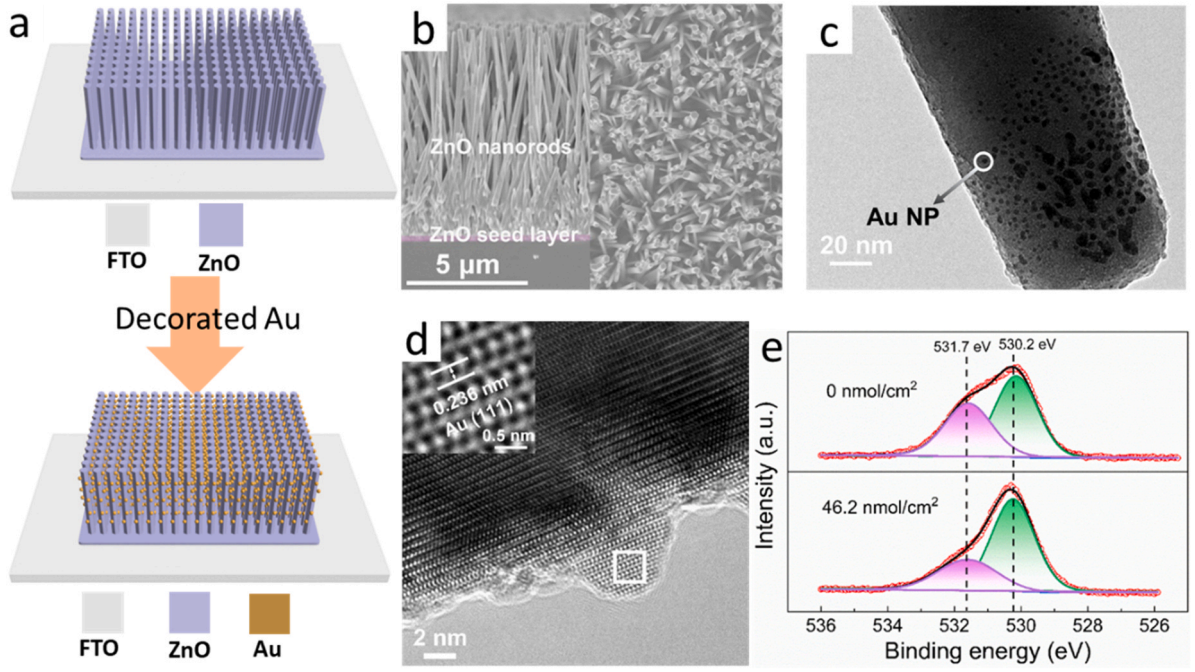

Fig. 1. Structure of materials and photodetector. (a) Schematic diagram of ZnO NWs befor and after decorating Au NPs. (b) Top-view and cross-section SEM image. (c) TEM image of Au NPs@ZnO (Loading amount of Au NPs is 46.2 nmol/cm^2). (d) HRTEM of Au NPs@ZnO corresponding to Fig. 1c. (e) O1s XPS spectra of ZnO NWs before and after decoorating Au NPs of 46.2 nmol/cm^2.

15.4 nmol/cm^2 and 107.9 nmol/cm^2 can be found (Fig. S4) in Supplementary data. The broad peak centered at 550 nm is related to defect-assisted emission of ZnO NWs. These defects mainly involve oxygen vacancies on the surface of ZnO [43,44]. After decorating Au NPs, the intensity of PL peak related to defect-assisted emission is weakened because of the reduction of the surface traps due to surface passivation effects by Au NPs [45–47]. PPC effect of ZnO NWs is related to oxygen vacancies [21]. Passivating the oxygen vacancy on the surface of ZnO NWs is beneficial to realize the fast response and recovery during light detection.

Under the illumination of 325 nm light with the power density of 68 nW/cm^2, the photoresponse of the self-powered photodetector with different loading amounts of Au NPs is shown in Fig. 2. The original device exhibits no response under the illumination of 325 nm light with the low power density of 68 nW/cm^2 (Fig. 2a). The feature of photoresponse emerges gradually with the increase of the loading amount of Au NPs. The notable photoresponse signal is observed for the photodetector after loading of Au NPs with 61.7 nmol/cm^2 even if the weak UV light illuminates. Photocurrent reaches the maximum value when the loading amount of Au NPs is 107.9 nmol/cm^2. Then, it decreases. The rise and fall time of device is obtained by measuring the *I-t* curve from Fig. 2a. The rise and fall time of photodetector after decorating Au NPs of 46.2 nmol/cm^2 are ~65 ms. Increasing the loading amount of Au NPs, the rise and fall time range from 30 ms to 42 ms (Fig. 2b). Responsivity and detectivity are crucial parameters to describe the performance of photodetector. Responsivity (R) and detectivity (D^*) are crucial parameters to describe the performance of photodetector. R and D^* are defined as:

$$R = \frac{I_{light} - I_{dark}}{P_{ill} S} \quad (1)$$

$$D^* = \frac{S^{1/2}R}{(2qI_{dark})} \quad (2)$$

where I_{light} and I_{dark} are the photocurrent and dark current, P_{ill} is the power density of incident light, S is the effective area of photodetector, q is the electron charge. We calculate to get them according to the *I-t* curve (Fig. 2a). Responsivity rises from zero to 0.485 mA/W (Fig. 2c). Detectivity (D^*) is also enhanced from zero to 27.49×10^{10} Jones (Fig. 2d). The phenomenon that the pyroelectric current of the photodetector with the loading amount of 123.3 nmol/cm^2 is decreased is observed. Extinction (absorption+scattering) cross-section of a metal nanosphere due to LSPR can be calculated by Mie theory [48]. The absorption cross-section and scattering cross-section can be determined by formula 1 and formula 2 in the supplementary material. If r < < λ (r is the radius of NP, λ is the wavelength of incident light), absorption is proportional to r^3, whereas scattering is proportional to r^6 [49]. From the bright field (Fig. 1e) and dark field (Fig. S3a), We can find that the abundant Au NPs on the surface of ZnO NWs result in the aggregation of Au NPs into the big particles, which leads to enhance scattering noticeably with a weak increase of absorption. In the case of photodetector after decorating Au NPs of 123.3 nmol/cm^2, the increase of reflectance also confirms this phenomenon (Fig. S5). In this case, the photothermal conversion will be decreased remarkably. Therefore, the pyroelectric current of the photodetector with the loading amount of 123.3 nmol/cm^2 decreases owing to the decrease of photothermal conversion.

The energy band structure of different materials is used to explain the contact state of the heterojunction interface. The similar conductive bands between FTO and ZnO endow them Ohmic contact. The high work function of Ag (4.64 eV) [50,51] comparing with the electron affinity of ZnO (4.35 eV) [2] makes the formation of Schottky contact (Fig. 3a). The *I-V* curve of the original device confirms a typical non-linear characteristic (Fig. 3b), indicating the formation of a Schottky junction between Ag and ZnO NWs. After decorating Au NPs on the surface of ZnO, absorption of ZnO after Au NPs decoration is enhanced compared with pure ZnO (Fig. 3c and Fig. 3g). Absorption is boosted with the increase of the loading

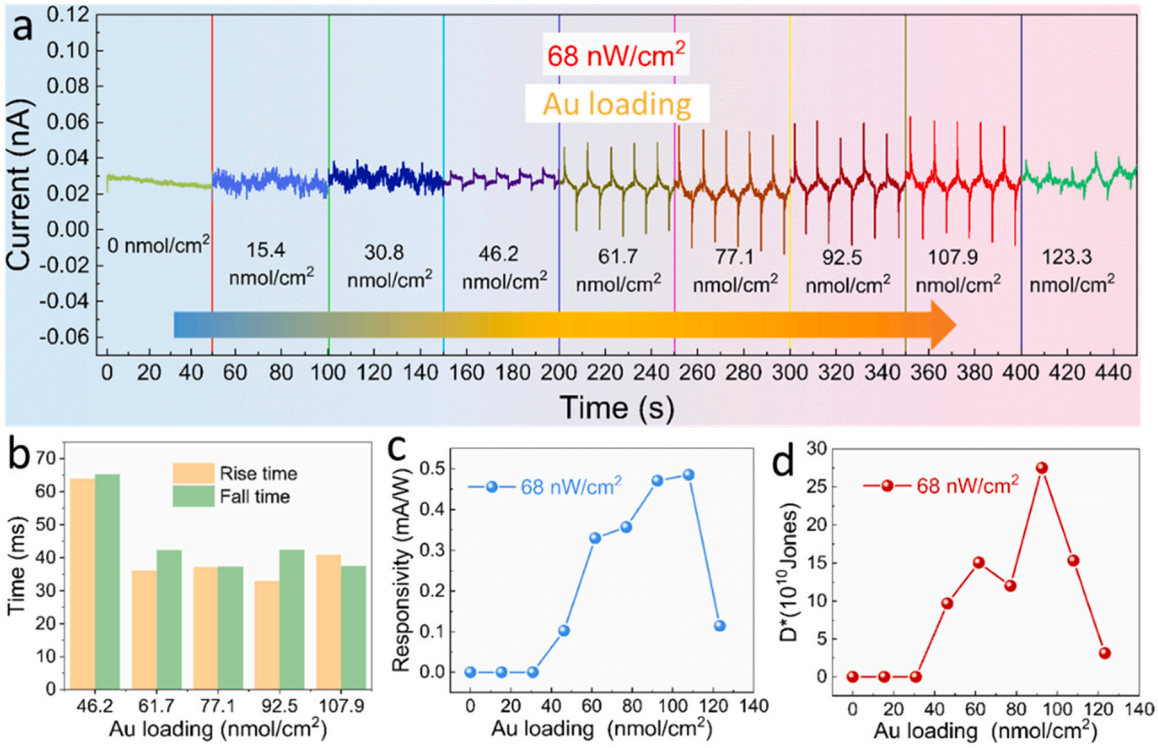

Fig. 2. Photoresponse performance of Schottky junction based on Au NPs@ZnO NW under the illumination of 325 nm light with power density of 68 nW/cm^2. (a) *I-t* dynamic response characteristics of device as a function of loading amount of Au NPs under 325 nm illuminations. (b) Rise and fall time of photodetector with different loading amounts of Au NPs. (c) Responsivity of photodetector with different loading amounts of Au NPs. (d) Detectivity of photodetector calculated from data of Fig. 2a.

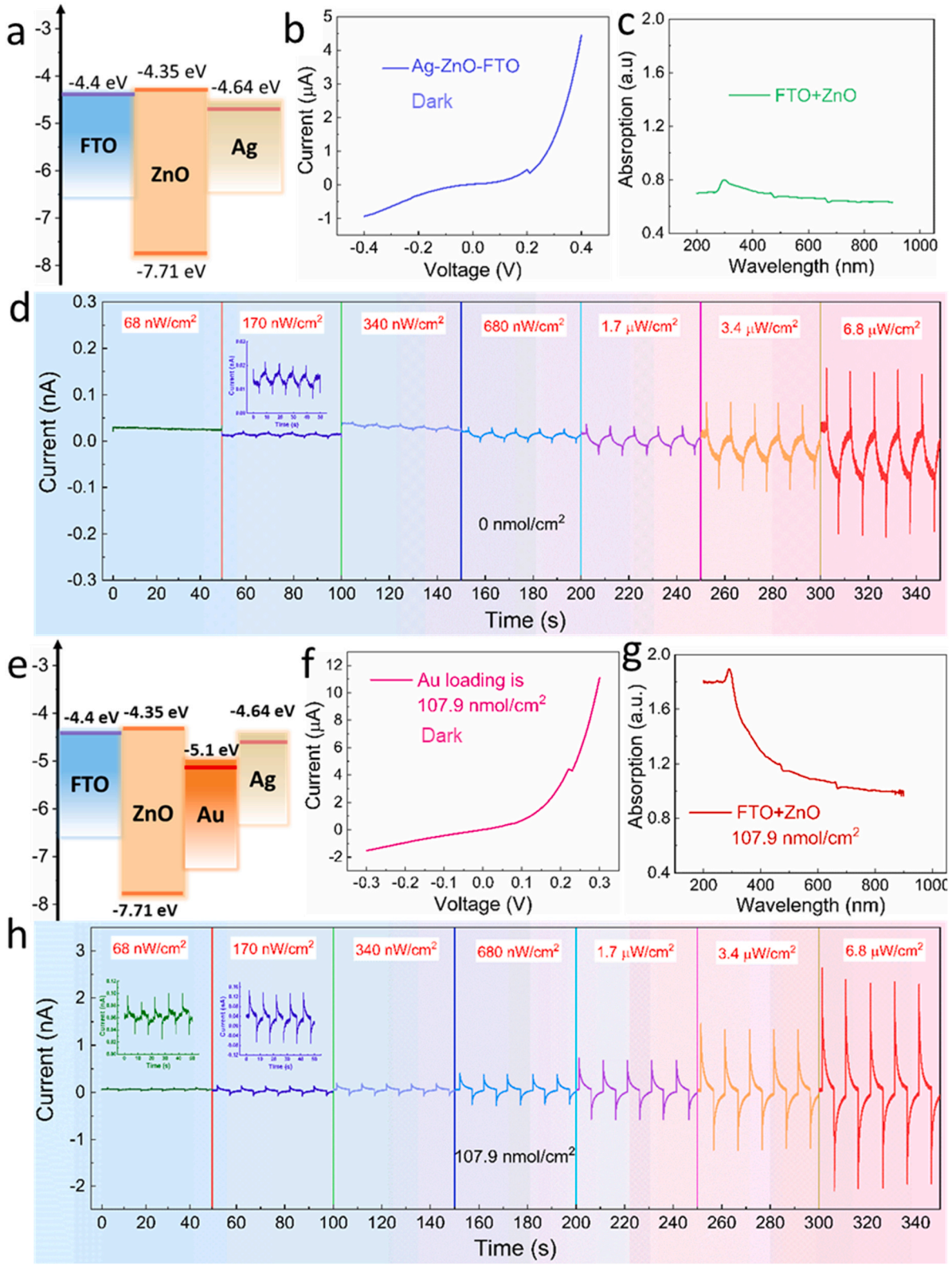

Fig. 3. Comparation of performance between original device and device based on Au NPs@ZnO NWs (107.9 nmol/cm^2). (a) Energy band of original device. (b) *I-V* curve of original device under dark condition. (c) Absorption of ZnO NWs growth on FTO. (d) *I-t* characteristics of original device under zero bias. (e) Energy band of device based on Au NPs@ZnO NWs. (f) *I-V* curve of device based on Au NPs@ZnO NWs (107.9 nmol/cm^2) under dark condition. (g) Absorption of ZnO NWs after decorating Au NPs of 107.9 nmol/cm^2. (h) *I-t* characteristics of device after decorating Au NPs (107.9 nmol/cm^2) under zero bias.

amount of Au NPs (Fig. S6). Devices still exhibit the non-linear *I-V* curve (Fig. 3f and Fig. S7), indicating the junction formed between Ag and Au NPs@ZnO NWs is still Schottky contact. From the energy band of the device after decorating Au NPs, the nano-Schottky junction will form because of the high work function of Au (5.1 eV) comparing with the electron affinity of ZnO (4.35 eV) (Fig. 3e). The deletion region around the interface of Au NPs and ZnO will reduce the carrier density in ZnO NWs, which is beneficial to suppress the dark current [52]. Additionally, plasmonic hot electrons generated from plasmonic dephasing can overcome Schottky barriers at metal/semiconductor interface and involve into the conductive band (CB) of semiconductor once the 325 nm light illuminates [42]. It will enhance the responsivity. The comparison of photoresponse is conducted between the original device and the device after decorating Au NPs. There is no photoresponse for the original device under the illumination of 325 nm light with the power density of 68 nW/cm^2 (Fig. 3d). The weak current signal is enhanced owing to the increase of power density. The current variation ($I_{pyro+photo}$-I_{dark}) is only 0.135 nA even if the original device is illuminated by 325 nm UV light with the power density of 6.8 μW/cm^2 (Fig. 3d). The notable photoresponse l can be captured for the device after decorating Au NPs of 107.9 nmol/cm^2 even if the weak light of 6.8 nW/cm^2 illuminates (Fig. 3h). Current variation ($I_{pyro+photo}$-I_{dark}) reaches 2.48 nA under the illumination of 325 nm laser with the power density of 6.8 μW/cm^2. It is about 18 times comparing with the corresponding performance of the original device. *Q-t* curve of photodetector after decorating Au NPs of 107.9 is used to verify the charge transfer of photodetector (Fig. S8). When the light is turned on or turned off, the charges are transferred quickly because they are driven by pyroelectric potential, then, the change transfer becomes slow. Additionally, the *V-t* curve of photodetector after decorating Au NPs of 107.9 nmol/cm^2 was also measured to confirm the change of voltage under the illumination of 325 nm light with the power density of 6.8 μW/cm^2 (Fig. S9). The open-circuit *V-t* curve exhibits the similar feature with *I-t* curve. The forward and reverse spike voltage, which is mainly owing to pyroelectric potential, can be observed at the moment of turning on/off light. The voltage from the photovoltaic effect, which shows a plateau, is emerged immediately. The potential generated by the pyroelectric effect and photovoltaic effect endows the self-powered nature of photodetector.

Besides the enhanced photoresponse for the 325 nm light with the low power density of 68 nW/cm^2, the performances of self-power photodetecor, including response time, recovery time, responsivity, and detectivity, are investigated under the illumination of 325 nm light with power density ranged from 68 nW/cm^2 to 6.8 μW/cm^2. Under the illumination of 325 nm light with the power density of 6.8 μW/cm^2, the rise and fall time of the original device is 21.38 ms and 22.31 ms, respectively. After decorating Au NPs of 61.7 nmol/cm^2, the rise time and fall time of the self-powered photodetector are 12.01 ms and 12.41 ms, respectively (Fig. 4a), they are improved remarkably. The pyroelectric potential is enhanced because of the increased of temperature change caused by LSPR effect. It is beneficial to shorten the response and recovery times [1]. Responsivity and detectivity are calculated to obtain through the *I-t* curve (Fig. S10). Responsivity is promoted as the increase of the loading amount of Au NPs at a fixed power density for 325 nm light (Fig. 4b). The saturation state is achieved when the loading amount of Au NPs is 107.9 nmol/cm^2. The phenomenon of decline for the device with the loading amount of 123.3 nmol/cm^2 is owing to the enhancement of scattering noticeably with a weak increase of absorption because of the aggregation of Au NPs. The maximum of responsivity reaches 0.664 mA/W for the device after decorating Au NPs of 107.9 nmol/cm^2 under the illumination of 325 nm light with the power density of 170 nW/cm^2. The ratio of responsivity between the original device

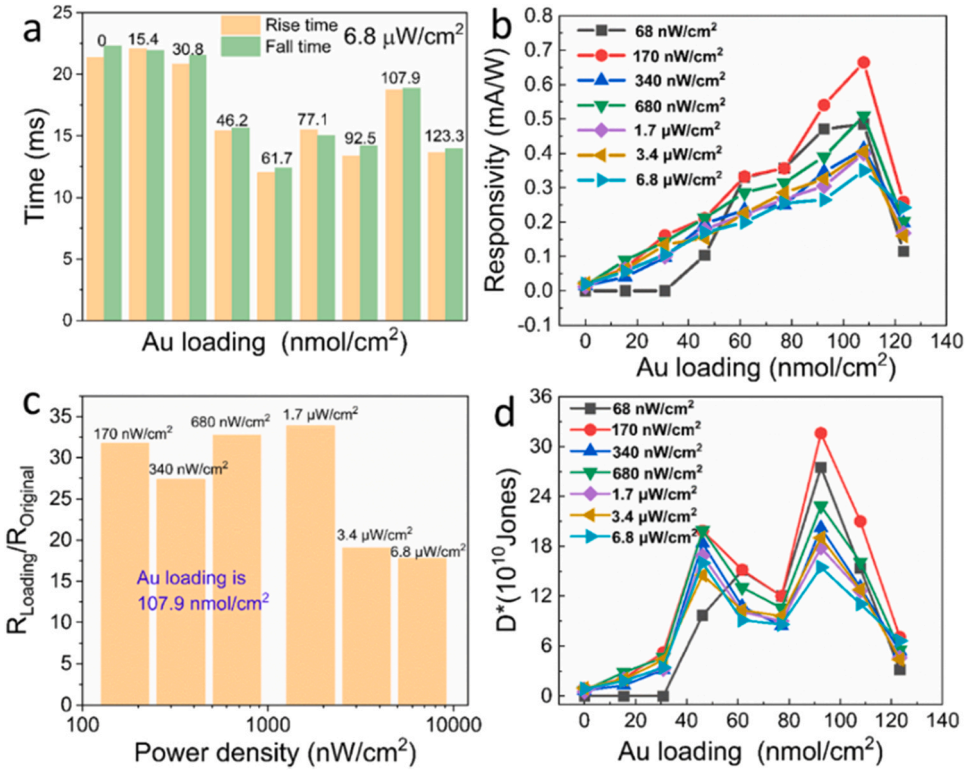

Fig. 4. Photoresponse performance of device before and after decorating Au NPs. (a) Rise and fall time under the illumination of 325 nm light with power density of 6.8 μW/cm^2. (b) Responsivity of device before and after decorating Au NPs as a function of power density of 325 nm light. (c) The ratio of responsivity ($R_{Loading}/R_{Original}$) between original device and device after decorating Au NPs (107.9 nmol/cm^2). (d) Detectivity of device before and after decorating Au NPs as a function of power density of 325 nm light.

and device after decorating Au NPs of 107.9 nmol/cm^2 is 17.8 at least under the illumination of 325 nm light with the power density ranging from 170 nW/cm^2 to 6.8 μW/cm^2 (Fig. 4c). The maximum value of the ratio attains to 33.9. The responsivity of self-powered photodetector after decorating Au NPs exhibits a significant improvement of over 3290% under the illumination of 325 nm light with the power density of 170 nW/cm^2. Detectivity of self-powered photodetector after decorating by Au NPs is also heightened remarkably comparing with the corresponding performance of the original photodetector (Fig. 4d). By decorating Au NPs of 92.5 nmol/cm^2, detectivity is enhanced from 0.93×10^{10} to 31.6×10^{10} Jones under the illumination of 325 nm light with the power density of 170 nW/cm^2, showing an improvement of 3298%, which exhibits the excellent performance among the previous reported ZnO-based UV photodetector (Table S1, Supplementary material). From the above performance, including rise/fall time, responsivity and detectivity, we can confirm that LSPR induced by Au NPs can enhance the performance of photodetection markedly.

The working mechanism of LSPR enhanced pyro-phototronic effect is unambiguously elaborated in Fig. 5. Schottky junction formed at the interface of Ag and ZnO induces energy band of ZnO around interface bends upward at the initial state (Fig. 5a). Once 325 nm light illuminates on a self-powered photodetector, the electron-hole pairs are generated by the photoexcitation process, increasing carrier concentration in ZnO. Carriers are separated to be detected by the built-in potential, realizing the self-powered detection. Additionally, temperature change triggered by light illumination inspires the pyroelectric effect of ZnO. Pyroelectric current is obtained from the release of bound charge attracted to the charged surfaces of the material mainly according to the primary pyroelectric effect [53]. The high-energy electrons generated by the strong oscillation of the surface electrons owing to LSPR effect are damped to the lattice by electron-vibration interactions, heating-up the lattice of Au NPs from the initial temperature to an equilibrium temperature. Then, the thermal energy transfers to ZnO NWs, which makes the huge transient change of temperature. Plasmon-heating effect can convert light energy into thermal energy and dissipate in ambient instantaneously within 100 ps [54,55]. The pyroelectric current is boosted because of the giant temperature change produced by LSPR of Au NPs instantaneously. Pyroelectric coefficient exhibits an increase when pyroelectric materials are heated below Curie temperature [53,56], which is ~ 342 K for ZnO by theoretical calculation [57]. Previous results indicates that pyroelectric coefcients of ZnO increases when heated below 430 K [58]. The temperature change enhanced by Au NPs are determined by finite difference time domain (FDTD) simulation (Fig. S11, Supplementary material). Plasmonic heat effect from LSPR will increase pyroelectric coefficient once 325 nm light illuminates. Additionally, a huge transient change of temperature leads to significant thermal deformation of the wurtzite ZnO crystal, which strengthens the pyroelectric potential along the *c*-axis direction of ZnO NWs prominently. Positive pyro-polarization charges at the interface of Ag and ZnO reduce the Schottky barrier height at the Ag-ZnO interface (Fig. 5b). Furthermore, plasmonic hot-electrons with higher energy than the Schottky barrier of Au and ZnO NWs can overcome the energy barrier at interface (inset in Fig. 5b) [59]. They can be involved into the conduction band of ZnO and enhance the photoresponse performance. The obvious photocurrent signals are detected even if under 325 nm light illuminations with ultralow power density. The temperature of different parts in ZnO NWs reaches the balance by heat conduction (Fig. 5c). Photocurrent realizes steady-state by photoexcitation process under continuous light illumination. The temperature at the top of ZnO decreases rapidly at the instant of turning off the light, which increases the spontaneous polarization of ZnO [53]. Pyroelectric current in the reverse direction is produced mainly from the primary pyroelectric effect. Besides, negative pyro-polarization charges generated by pyroelectric potential will increase barrier height (Fig. 5d), which tunes the carrier separation, transportation, and diffusion.

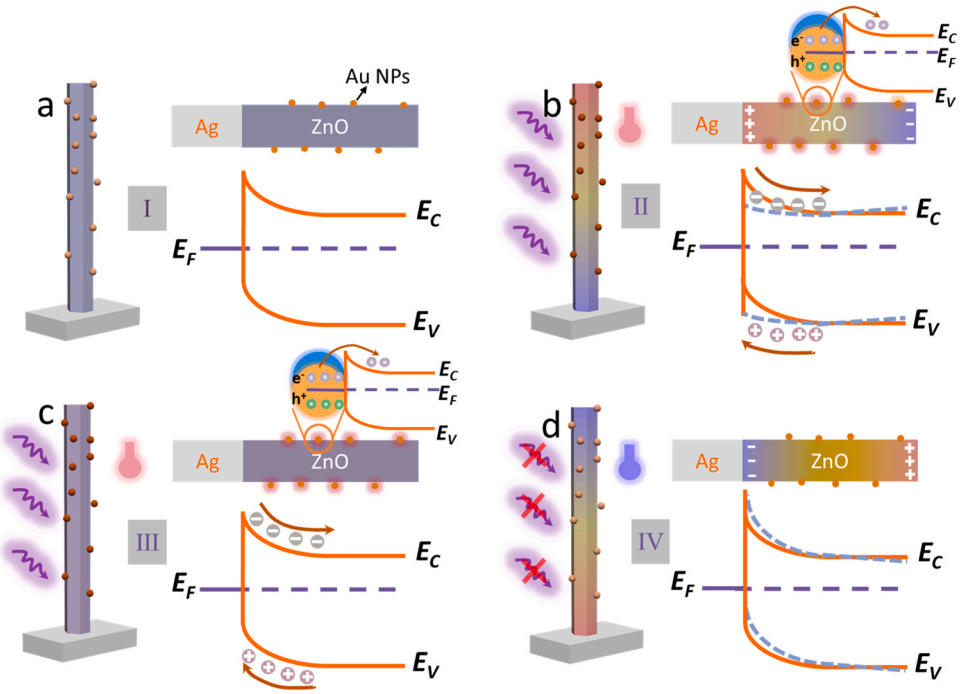

Fig. 5. Working mechanism of self-powered photodetector based on Schottky junction of Au NPs@ZnO NWs combined with LSPR and pyroelectric effect. (a-d) Energy band diagram of Schottky junction under different condition. (a) at dark. (b) the moment of turning on light. (c) continuous illumination. (d) the moment of turning off light.

Conclusion

We demonstrate a self-powered photodetector for ultralow power density UV sensing by LSPR-enhanced pyro-phototronic effect in a Schottky junction based on Au NPs@ZnO NWs. The LSPR-induced pyro-phototronic effect can effectively tune the Schottky barrier height and the distribution of electric field at the interface, thus, enhancing photoresponse and shortening the response and recovery time. The self-powered photodetector achieves highly sensitive UV detection even if the power density is as low as 68 nW/cm^2 by decorating Au NPs on the surface of ZnO NWs. After decorating Au of 107.9 nmol/cm^2, responsivity and detectivity attain 0.485 mA/W and 27.49×10^{10} Jones for the self-powered photodetector under the illumination of 325 nm light with the power density of 68 nW/cm^2, whereas the original device has no response. The responsivity and detectivity of self-powered photodetector after decorating Au NPs exhibits a significant improvement of over 3290% and over 3298% under the illumination of 325 nm light with the power density of 170 nW/cm^2. Fast recovery ensures detection is finished within ~12 ms. The working mechanism based on the energy band diagram is proposed to explain the observed performance of self-powered photodetector. This self-powered photodetector utilized the advantage of plasmonic heat effect, hot electron injection, and LSPR-enhanced pyro-phototronic effect. The discovery and inspiration in this work could be the cornerstone for designing high-performance photodetectors using other nanomaterials. The designed photodetector of prominent comprehensive performance has potential application in military and civilian fields, including military warning, space science, flame sensing, life science, optical communication/imaging.

Experimental section

Fabrication of Schottky junction PDs based on Au NPs@ZnO and Ag: ZnO NWs were prepared by hydrothermal method. First, FTO-coated glass was cleaned with acetone and ethanol sonication. Then, a thin seed layer of ZnO was deposited on FTO-coated glass by radio frequency magnetron sputtering (Denton Discovery 635). The substrate with seed layer was immersed into the solution at 90 ºC for 8 h to grow ZnO NWs. The solution contained 20 mM zinc nitrate ($Zn(NO_3)_2.6H_2O$), 20 mM hexamethylenetetramine (HMTA) and 5 vol% ammonium hydroxide (NH_4OH). Then, ZnO NWs were cleaned with deionized water. Au NPs were deposited on the surface of ZnO NWs by sputtering (108Auto sputter coater). The area of ZnO NWs after decorated Au NPs is about 1×1 cm^2. The loading amount of Au NPs was obtained by measuring the mass difference before and after depositing on sapphire substrate with the diameter of 50 mm. A thin layer of Ag was deposited to form the Schottky junction. Two conducting wires were fixed on the FTO and Ag electrode by silver paste.

Materials characterize: Surface and cross-section morphologies were characterized by SEM (Hitachi SU8020). XRD pattern was used to confirm the phase structure by using X-ray diffractometer (PANalytical X`Pert) with Cu kα source (λ = 0.154 nm). Microstructure and composition of ZnO and Au NPs@ZnO were obtained by TEM method (Tecnai G^2 F20).

Optical and Electrical Measurements: UV-Vis-NIR spectrophotometer was used to determine the absorptance of ZnO before and after decorating Au NPs. The binding energy of O 1 s was analyzed by X-ray photoelectron spectroscopy (XPS, ESCALAB 250Xi, Thermo Fisher). PL spectra excited by 325 nm He-Cd laser (LabRAM HR Evolution, Horiba) was used to characterize the defect related to oxygen vacancy. *I-V* curve of the device was measured by a semiconductor analysis system (Keithley 4200-SCS). Photoresponse current was recorded by using a Keithley 6517 system. Data were collected by using a Tektronix oscilloscope (HD06104). Optical input stimuli were provided by a He-Cd laser (Model No. KI5751I-G, Kimmon Koha Co., Ltd.). A filter was used to change the light power density. A UV objective lens was placed to expand the laser. The area of UV illumination covered the whole photodetector. The interactive area between UV light and PDs is 1 cm × 1 cm. Power density was measured by a digital powermeter (Thorlab PM100D and Newport 818 P-001-12).

CRediT authorship contribution statement

Jianping Meng: Conceptualization, Investigation, Methodology, Writing – original draft, Data curation, Validation, Funding acquisition. **Qi Li:** Investigation, Data curation. **Jing Huang:** Investigation. **Caofeng Pan:** Writing – review & editing. **Zhou Li:** Supervision, Resources, Funding acquisition, Writing – review & editing. All authors writing- review & editing.

Declaration of Competing Interest

The authors declare that they have no known competing financial interests or personal relationships that could have appeared to influence the work reported in this paper.

Acknowledgements

The authors are thankful for the support provided by the National Natural Science Foundation of China (52002027, T2125003, 61875015), the Natural Science Foundation of Beijing Municipality (2214083, JQ20038, L212010), and the Youth Backbone Individual Project of Beijing Excellent Talents Training (Y9QNGG0501).

Appendix A. Supporting information

Supplementary data associated with this article can be found in the online version at doi:10.1016/j.nantod.2022.101399.

References

[1] Y. Wang, L.P. Zhu, Y.J. Feng, Z.N. Wang, Z.L. Wang, Comprehensive pyro-phototronic effect enhanced ultraviolet detector with ZnO/Ag schottky junction, Adv. Funct. Mater. 29 (2019) 1807111, https://doi.org/10.1002/adfm.201807111
[2] Z.N. Wang, R.M. Yu, C.F. Pan, Z.L. Li, J. Yang, F. Yi, Z.L. Wang, Light-induced pyroelectric effect as an effective approach for ultrafast ultraviolet nanosensing, Nat. Commun. 6 (2015) 8401, https://doi.org/10.1038/ncomms9401
[3] K.S. Pasupuleti, M. Reddeppa, B.G. Park, J.E. Oh, S.G. Kim, M.D. Kim, Phys. Status Solidi-R. (2021), https://doi.org/10.1002/pssr.202000518
[4] M. Reddeppa, B.G. Park, K.S. Pasupuleti, D.J. Nam, S.G. Kim, J.E. Oh, M.D. Kim, Current–voltage characteristics and deep-level study of GaN nanorod Schottky-diode-based photodetector, Semicond. Sci. Technol. 36 (2021) 035010, https://doi.org/10.1088/1361-6641/abda62
[5] B.D. Boruah, Zinc oxide ultraviolet photodetectors: rapid progress from conventional to self-powered photodetectors, Nanoscale Adv. 1 (2019) 2059–2085, https://doi.org/10.1039/c9na00130a
[6] T.Y. Zhai, X.S. Fang, M.Y. Liao, X.J. Xu, H.B. Zeng, B. Yoshio, D. Golberg, A comprehensive review of one-dimensional metal-oxide nanostructure photodetectors, Sensors 9 (2009) 6504–6529, https://doi.org/10.3390/s90806504
[7] C. Soci, A. Zhang, B. Xiang, S.A. Dayeh, D.P.R. Aplin, J. Park, X.Y. Bao, Y.H. Lo, D. Wang, ZnO nanowire UV photodetectors with high internal gain, Nano Lett. 7 (2007) 1003–1009, https://doi.org/10.1021/nl070111x
[8] X. Liu, L.L. Gu, Q.P. Zhang, J.Y. Wu, Y.Z. Long, Z.Y. Fan, Nat. Commun. 5 (2014) 1–9, https://doi.org/10.1038/ncomms5007
[9] B. Zhao, F. Wang, H. Chen, L. Zheng, L. Su, D. Zhao, X. Fang, An ultrahigh responsivity (9.7 mA W−1) self-powered solar-blind photodetector based on individual ZnO–Ga_2O_3heterostructures, Adv. Funct. Mater. 27 (2017) 1700264, https://doi.org/10.1002/adfm.201700264
[10] J.P. Meng, H. Li, L.M. Zhao, J.F. Lu, C.F. Pan, Y. Zhang, Z. Li, Triboelectric nanogenerator enhanced schottky nanowire sensor for highly sensitive ethanol detection, Nano Lett. 20 (2020) 4968–4974, https://doi.org/10.1021/acs.nanolett.0c01063
[11] W.B. Peng, X.F. Wang, R.M. Yu, Y.J. Dai, H.Y. Zou, A.C. Wang, Y.N. He, Z.L. Wang, Enhanced performance of a self-powered organic/inorganic photodetector by pyro-phototronic and piezo-phototronic effects, Adv. Mater. 29 (2017) 1606698, https://doi.org/10.1002/adma.201606698
[12] Y. Chen, L. Su, M. Jiang, X. Fang, Switch type PANI/ZnO core-shell microwire heterojunction for UV photodetection, J. Mater. Sci. Technol. 105 (2022) 259–265, https://doi.org/10.1016/j.jmst.2021.07.031

[13] Q. Li, J.P. Meng, J. Huang, Z. Li, Plasmon-induced pyro-phototronic effect enhancement in self-powered uv–vis detection with a zno/cuo p–n junction device, Adv. Funct. Mater. (2021) 2108903, https://doi.org/10.1002/adfm.202108903

[14] J. Zhou, Y.D. Gu, Y.F. Hu, W.J. Mai, P.H. Yeh, G. Bao, A.K. Sood, D.L. Polla, Z.L. Wang, Gigantic enhancement in response and reset time of ZnO UV nanosensor by utilizing schottky contact and surface functionalization, Appl. Phys. Lett. 94 (2009) 191103, https://doi.org/10.1063/1.3133358

[15] B.A. Nie, J.G. Hu, L.B. Luo, C. Xie, L.H. Zeng, P. Lv, F.Z. Li, J.S. Jie, M. Feng, C.Y. Wu, Y.Q. Yu, S.H. Yu, Monolayer graphene film on ZnO nanorod array for high-performance Schottky junction ultraviolet photodetectors, Small 9 (2013) 2872–2879, https://doi.org/10.1002/smll.201203188

[16] S.N. Lu, J.J. Qi, S. Liu, Z. Zhang, Z.Z. Wang, P. Lin, Q.L. Liao, Q.J. Liang, Y. Zhang, Piezotronic interface engineering on ZnO/Au-based Schottky junction for enhanced photoresponse of a flexible self-powered UV detector, ACS Appl. Mater. Interface 6 (2014) 14116–14122, https://doi.org/10.1021/am503442c

[17] M.J. Dai, H.Y. Chen, F.K. Wang, M.S. Long, H.M. Shang, Y.X. Hu, W. Li, C.Y. Ge, J. Zhang, T.Y. Zhai, Y.Q. Fu, P.A. Hu, Ultrafast and sensitive self-powered photodetector featuring self-limited depletion region and fully depleted channel with van der waals contacts, ACS Nano 14 (2020) 9098–9106, https://doi.org/10.1021/acsnano.0c04329

[18] W. Ouyang, J. Chen, Z. Shi, X. Fang, Self-powered UV photodetectors based on ZnO nanomaterials, Appl. Phys. Rev. 8 (2021) 031315, https://doi.org/10.1063/5.0058482

[19] V.H. Vuong, S.V.N. Pammi, K.S. Pasupuleti, W.G. Hu, V.D. Tran, J.S. Jung, M.D. Kim, V. Pecunia, S.G. Yoon, Engineering chemical vapor deposition for lead-free perovskite-inspired ma3bi2i9self-powered photodetectors with high performance and stability, Adv. Opt. Mater. 9 (2021) 2100192, https://doi.org/10.1002/adom.202100192

[20] S. Jeon, S.E. Ahn, I. Song, C.J. Kim, U.I. Chung, E. Lee, I. Yoo, A. Nathan, S. Lee, J. Robertson, K. Kim, Gated three-terminal device architecture to eliminate persistent photoconductivity in oxide semiconductor photosensor arrays, Nat. Mater. 11 (2012) 301–305, https://doi.org/10.1038/Nmat3256

[21] S. Lany, A. Zunger, Anion vacancies as a source of persistent photoconductivity in II-VI and chalcopyrite semiconductors, Phys. Rev. B 72 (2005) 035215, https://doi.org/10.1103/PhysRevB.72.035215

[22] A. Janotti, C.G. Van de Walle, Native point defects in ZnO, Phys. Rev. B 76 (2007) 165202, https://doi.org/10.1103/PhysRevB.76.165202

[23] F. Oba, A. Togo, I. Tanaka, J. Paier, G. Kresse, Defect energetics in ZnO: a hybrid Hartree-Fock density functional study, Phys. Rev. B 77 (2008) 245202, https://doi.org/10.1103/PhysRevB.77.245202

[24] Z.Y. Han, H.L. Liang, W.X. Huo, X.S. Zhu, X.L. Du, Z.X. Mei, Adv. Opt. Mater. 8 (2020), https://doi.org/10.1002/adom.201901833

[25] P. Feng, I. Monch, S. Harazim, G.S. Huang, Y.F. Mei, O.G. Schmidt, Giant persistent photoconductivity in rough silicon nanomembranes, Nano Lett. 9 (2009) 3453–3459, https://doi.org/10.1021/nl9016557

[26] Y.K. Su, S.M. Peng, L.W. Ji, C.Z. Wu, W.B. Cheng, C.H. Liu, Ultraviolet ZnO nanorod photosensors, Langmuir 26 (2010) 603–606, https://doi.org/10.1021/la902171j

[27] Z.X. Xu, Y.L. Zhang, Z.N. Wang, ZnO-based photodetector: from photon detector to pyro-phototronic effect enhanced detector, J. Phys. D: Appl. Phys. 52 (2019) 223001, https://doi.org/10.1088/1361-6463/ab0728

[28] X.F. Wang, Y.J. Dai, R.Y. Liu, X. He, S.T. Li, Z.L. Wang, Light-triggered pyroelectric nanogenerator based on a pn-junction for self-powered near-infrared photosensing, ACS Nano 11 (2017) 8339–8345, https://doi.org/10.1021/acsnano.7b03560

[29] J.P. Meng, Z. Li, Schottky-contacted nanowire sensors, Adv. Mater. 32 (2020) 2000130, https://doi.org/10.1002/adma.202000130

[30] J.Q. Dong, Z.J. Wang, X.F. Wang, Z.L. Wang, Temperature dependence of the pyro-phototronic effect in self-powered p-Si/n-ZnO nanowires heterojuncted ultraviolet sensors, Nano Today 29 (2019) 100798, https://doi.org/10.1016/j.nantod.2019.100798

[31] S. Podder, B. Basumatary, D. Gogoi, J. Bora, A.R. Pal, Pyro-phototronic application in the Au/ZnO interface for the fabrication of a highly responsive ultrafast UV photodetector, Appl. Surf. Sci. 537 (2021) 147893, https://doi.org/10.1016/j.apsusc.2020.147893

[32] W.B. Peng, R.M. Yu, X.F. Wang, Z.N. Wang, H.Y. Zou, Y.N. He, Z.L. Wang, Temperature dependence of pyro-phototronic effect on self-powered ZnO/perovskite heterostructured photodetectors, Nano Res. 9 (2016) 3695–3704, https://doi.org/10.1007/s12274-016-1240-5

[33] M. Rycenga, C.M. Cobley, J. Zeng, W.Y. Li, C.H. Moran, Q. Zhang, D. Qin, Y.N. Xia, Controlling the synthesis and assembly of silver nanostructures for plasmonic applications, Chem. Rev. 111 (2011) 3669–3712, https://doi.org/10.1021/cr100275d

[34] X.L. Zhang, Q.Y. Liu, B.D. Liu, W.J. Yang, J. Li, P.J. Niu, X. Jiang, Giant UV photoresponse of a GaN nanowire photodetector through effective Pt nanoparticle coupling, J. Mater. Chem. C. 5 (2017) 4319–4326, https://doi.org/10.1039/c7tc00594f

[35] X. Zhao, F. Wang, L.L. Shi, Y.P. Wang, H.F. Zhao, D.X. Zhao, Performance enhancement in ZnO nanowire based double Schottky-barrier photodetector by applying optimized Ag nanoparticles, RSC Adv. 6 (2016) 4634–4639, https://doi.org/10.1039/c5ra20161f

[36] J.P. Meng, Mater. Today Phys. 9 (2019) 100131, https://doi.org/10.1016/j.mtphys.2019.100131

[37] K.S. Pasupuleti, M. Reddeppa, B.-G. Park, K.R. Peta, J.-E. Oh, S.-G. Kim, M.-D. Kim, Ag nanowire-plasmonic-assisted charge separation in hybrid heterojunctions of Ppy-PEDOT:PSS/GaN nanorods for enhanced UV photodetection, ACS Appl. Mater. Interfaces 12 (2020) 54181–54190, https://doi.org/10.1021/acsami.0c16795

[38] E.C. Garnett, W.S. Cai, J.J. Cha, F. Mahmood, S.T. Connor, M.G. Christoforo, Y. Cui, M.D. McGehee, M.L. Brongersma, Self-limited plasmonic welding of silver nanowire junctions, Nat. Mater. 11 (2012) 241–249, https://doi.org/10.1038/Nmat3238

[39] Z.J. Zhang, L.M. Wang, J. Wang, X.M. Jiang, X.H. Li, Z.J. Hu, Y.H. Ji, X.C. Wu, C.Y. Chen, Mesoporous silica-coated gold nanorods as a light-mediated multifunctional theranostic platform for cancer treatment, Adv. Mater. 24 (2012) 1418–1423, https://doi.org/10.1002/adma.201104714

[40] H.A. Atwater, A. Polman, Plasmonics for improved photovoltaic devices, Nat. Mater. 9 (2010) 205–213, https://doi.org/10.1038/Nmat2629

[41] C. Clavero, Plasmon-induced hot-electron generation at nanoparticle/metal-oxide interfaces for photovoltaic and photocatalytic devices, Nat. Photonics 8 (2014) 95–103, https://doi.org/10.1038/nphoton.2013.238

[42] H.B. Tang, C.J. Chen, Z.L. Huang, J. Bright, G.W. Meng, R.S. Liu, N.Q. Wu, Plasmonic hot electrons for sensing, photodetection, and solar energy applications: a perspective, J. Chem. Phys. 152 (2020) 220901, https://doi.org/10.1063/5.0005334

[43] Z.G. Geng, X.D. Kong, W.W. Chen, H.Y. Su, Y. Liu, F. Cai, G.X. Wang, J. Zeng, Oxygen vacancies in ZnO nanosheets enhance CO_2 electrochemical reduction to CO, Angew. Chem. Int. Ed. 57 (2018) 6054–6059, https://doi.org/10.1002/anie.201711255

[44] M. Baek, D. Kim, K. Yong, Simple but effective way to enhance photoelectrochemical solar-water-splitting performance of ZnO nanorod arrays: charge-trapping Zn(OH)2 annihilation and oxygen vacancy generation by vacuum annealing, ACS Appl. Mater. Interfaces 9 (2017) 2317–2325, https://doi.org/10.1021/acsami.6b12555

[45] C.W. Cheng, E.J. Sie, B. Liu, C.H.A. Huan, T.C. Sum, H.D. Sun, H.J. Fan, A comparative study of online suicide-related information in Chinese and English, Appl. Phys. Lett. 96 (2010) 313–319 https://doi.org/Artn 07110710.1063/1.3323091.

[46] T. Dixit, I.A. Palani, V. Singh, Role of surface plasmon decay mediated hot carriers toward the photoluminescence tuning of metal-coated ZnO nanorods, J. Phys. Chem. C. 121 (2017) 3540–3548, https://doi.org/10.1021/acs.jpcc.6b11526

[47] W.Z. Liu, H.Y. Xu, C.L. Wang, L.X. Zhang, C. Zhang, S.Y. Sun, J.G. Ma, X.T. Zhang, J.N. Wang, Y.C. Liu, Enhanced ultraviolet emission and improved spatial distribution uniformity of ZnO nanorod array light-emitting diodes via Ag nanoparticles decoration, Nanoscale 5 (2013) 8634–8639, https://doi.org/10.1039/c3nr02844e

[48] P. Mulvaney, Surface plasmon spectroscopy of nanosized metal particles, Langmuir 12 (1996) 788–800, https://doi.org/10.1021/la9502711

[49] C. Langhammer, B. Kasemo, I. Zoric, Absorption and scattering of light by Pt, Pd, Ag, and Au nanodisks: absolute cross sections and branching ratios, J. Chem. Phys. 126 (2007) 194702, https://doi.org/10.1063/1.2734550

[50] K.W. Zhang, Z.L. Wang, Y. Yang, Enhanced P_3HT/ZnO nanowire array solar cells by pyro-phototronic effect, ACS Nano 10 (2016) 10331–10338, https://doi.org/10.1021/acsnano.6b06049

[51] H.L. Skriver, N.M. Rosengaard, Surface energy and work function of elemental metals, Phys. Rev. B 46 (1992) 7157–7168, https://doi.org/10.1103/PhysRevB.46.7157

[52] N.S. Ramgir, P.K. Sharma, N. Datta, M. Kaur, A. Debnath, D. Aswal, S. Gupta, Room temperature H_2S sensor based on Au modified ZnO nanowires, Sens. Actuators B 186 (2013) 718–726.

[53] C.R. Bowen, J. Taylor, E. LeBoulbar, D. Zabek, A. Chauhan, R. Vaish, Energy Environ. Sci. 7 (2014) 3836–3856, https://doi.org/10.1039/c4ee01759e

[54] A. Crut, P. Maioli, N. Del Fatti, F. Vallee, Acoustic vibrations of metal nano-objects: time-domain investigations, Phys. Rep. 549 (2015) 1–43, https://doi.org/10.1016/j.physrep.2014.09.004

[55] Y.C. Zhang, S. He, W.X. Guo, Y. Hu, J.W. Huang, J.R. Mulcahy, W.D. Wei, Surface-plasmon-driven hot electron photochemistry, Chem. Rev. 118 (2018) 2927–2954, https://doi.org/10.1021/acs.chemrev.7b00430

[56] N. Ma, Y. Yang, Enhanced self-powered UV photoresponse of ferroelectric $BaTiO_3$ materials by pyroelectric effect, Nano Energy 40 (2017) 352–359, https://doi.org/10.1016/j.nanoen.2017.08.043

[57] T. Dietl, H. Ohno, F. Matsukura, J. Cibert, D. Ferrand, Zener model description of ferromagnetism in zinc-blende magnetic semiconductors, Science 287 (2000) 1019–1022, https://doi.org/10.1126/science.287.5455.1019

[58] G. Heiland, H. Ibach, Pyroelectricity of zinc oxide, Solid State Commun. 4 (1966) 353–356, https://doi.org/10.1016/0038-1098(66)90187-6

[59] H. Tang, C.-J. Chen, Z. Huang, J. Bright, G. Meng, R.-S. Liu, N. Wu, Plasmonic hot electrons for sensing, photodetection, and solar energy applications: a perspective, J. Chem. Phys. 152 (2020) 220901, https://doi.org/10.1063/5.0005334